Published in final edited form as:
J Neurol Sci. 2012 February 15; 313(1-2): 99–109. doi:10.1016/j.jns.2011.09.015.

Human Brain Atlas-based Multimodal MRI Analysis of Volumetry, Diffusimetry, Relaxometry and Lesion Distribution in Multiple Sclerosis Patients and Healthy Adult Controls: Implications for understanding the Pathogenesis of Multiple Sclerosis and Consolidation of Quantitative MRI Results in MS

Khader M. Hasan[*,1], **Indika S. Walimuni**[1], **Humaira Abid**[1], **Sushmita Datta**[1], **Jerry S. Wolinsky**[2], and **Ponnada A. Narayana**[1]

[1]Department of Diagnostic & Interventional Imaging, The University of Texas Health Science Center at Houston, 6431 Fannin Street, MSB 2.100, Houston, Texas 77030

[2]Department of Neurology, The University of Texas Health Science Center at Houston, 6431 Fannin Street, MSB 2.100, Houston, Texas 77030

Abstract

Multiple sclerosis (MS) is the most common immune-mediated disabling neurological disease of the central nervous system. The pathogenesis of MS is not fully understood. Histopathology implicates both demyelination and axonal degeneration as the major contributors to the accumulation of disability. The application of several *in vivo* quantitative magnetic resonance imaging (MRI) methods to both lesioned and normal-appearing brain tissue has not yet provided a solid conclusive support of the hypothesis that MS might be a diffuse disease.

In this work, we adopted FreeSurfer to provide standardized macrostructure or volumetry of lesion free normal-appearing brain tissue in combination with multiple quantitative MRI metrics (T_2 relaxation time, diffusion tensor anisotropy and diffusivities) that characterize tissue microstructural integrity. By incorporating a large number of healthy controls, we have attempted to separate the natural age-related change from the disease-induced effects. Our work shows elevation in diffusivity and relaxation times and reduction in volume in a number of normal-appearing white matter and gray matter structures in relapsing-remitting multiple sclerosis patients. These changes were related in part with the spatial distribution of lesions. The whole brain lesion load and age-adjusted expanded disability status score showed strongest correlations in regions such as corpus callosum with qMRI metrics that are believed to be specific markers of

[*]**Corresponding Author**: Khader M. Hasan, Ph.D., Fannin Street MSB 2.100, Houston TX 77030, TEL: (713) 500-7690; FAX: (713) 500-7684, Khader.M.Hasan@uth.tmc.edu .

[*]This work is presented in Abstract form two ISMRM2011 Presentations (Talk & ePoster):
Hasan, K.M,, Walimuni, I.S., Abid, H., Datta, S., Nelson, F., Wolinsky, J.S., Narayana, P.A., 2011. Atlas-based Quantification of Brain Normal-Appearing White and Gray Matter Volume, Relaxation Time and Diffusion Tensor Metrics in Multiple Sclerosis. 19th Annual Meeting and Exhibition of International Society for Magnetic Resonance in Medicine May 7-13, Montréal, Québec, Canada; #4482.
Hasan, K.M,, Walimuni, I.S., Abid, H., Datta, S., Nelson, F., Wolinsky, J.S., Narayana, P.A., 2011; Brain Atlas-based Lesion Spatial Distribution and Modeling of Wallerian Degeneration In Multiple Sclerosis 19th Annual Meeting and Exhibition of International Society for Magnetic Resonance in Medicine 7-13 May, Montréal, Québec, Canada; #4617.

axonal dysfunction, consistent with histologic data of others indicating axonal loss that is independent of focal lesions. Our results support that MS at least in part has a neurodegenerative component.

Keywords

brain atlas; FreeSurfer; qMRI; RRMS; DTI; T_2 relaxation; natural aging; neurodegeneration; axonal loss; demyelination; lesion maps

1. Introduction

The hallmarks of multiple sclerosis (MS) pathology include inflammation [1], demyelination [2], axonal loss [3], vascular abnormalities [4, 5], iron accumulation [6], mitochondrial dysfunction [7] and changes in cellular membrane permeability and sodium channels [8]. Histopathology has provided evidence for both lesion-centered inflammatory and neuronal-axonal injury in normal-appearing brain tissue (NABT) that appears independent from focal lesions [9].

In the past 30 years [10, 11], *in vivo* quantitative magnetic resonance imaging (qMRI) has provided important surrogate markers of MS disease progression [12], but no single MRI modality can provide specific information about the pathological hallmarks of MS [13]. Due to the adoption of different analysis approaches such as whole brain histogram, region-of-interest [14, 15, 16], fiber tractography [17], voxel-based [18], tensor-based morphometry [19], volume-based [20, 21] and the focus on certain tissue types such as gray or white matter in most previous studies, it is not clear how one can consolidate the published qMRI literature on MS.

Taken together qMRI studies provide a somewhat scattered evidence of a widespread generalized or diffuse pathology in different MS phenotypes [12, 22-24]. To the best of our knowledge, there has been no single consolidating *in vivo* MRI work in MS that adopted a comprehensive brain atlas of subcortical and cortical gray matter (GM) and white matter (WM) have been analyzed using macrostructure (e.g. volume) and corresponding microstructural or integrity attributes such as proton density, relaxation time, diffusion tensor-based measures such as anisotropy, mean, axial and radial diffusivities.

We sought to generalize our past multi-modal qMRI approach on the manually-delineated caudate nuclei in controls and MS patients [20] by obtaining subcortical or deep gray matter (DGM), cortex, deep WM (e.g. corpus callosum, periventricular WM), and lobar WM volumes automatically using FreeSurfer [25] which was validated [26] and used previously in MS [21, 27, 28].

The primary goal of this work was to test the hypothesis that MS pathology in normal-appearing cerebral tissue may be widespread [12, 22-24] using a host of qMRI metrics derived from multimodal methods and accounting for natural aging [20, 29] and pathology-driven neurodegenerative changes [20, 30]. We also investigated the interplay between qMRI metrics, whole brain lesions and disability to examine the possibility of separating direct lesion-related injury from age-independent neurodegenerative neuronal or axonal loss. This was realized by fusing T_2 relaxation time, proton density, lesion and diffusion tensor imaging (DTI) derived maps with FreeSurfer atlas-based volumetry.

2. Subjects and Methods

2.1 Study Population

The MRI protocol was approved by our Institutional Review Board (IRB). Written informed consent was obtained from each subject. Fifty four (15 men and 39 women) relapsing-remitting MS patients aged = 41.7 ± 9.6 years (mean ± standard deviation; see Table 1). At the time of their imaging session, 47% of RRMS patients were using glatiramer acetate, ~ 22% an interferon beta preparation (73.7% a subcutaneous product), as their disease modifying therapy (DMT) and ~ 25% were not receiving any DMT. In addition, 88 healthy adult controls (41 men and 47 women) aged = 37.9 ± 10.1 years (see Table 1) were recruited from the local community and university staff. All control subjects were screened for history of trauma, surgery, chronic illness, alcohol and/or drug abuse, neurological illness, and current pregnancy. None of the controls in this study reported any neurological conditions and their fluid-attenuated inversion recovery (FLAIR) conventional MRI data were judged to be normal

2.2 MRI Data Acquisition

All MRI studies were performed on a 3.0 T Philips Intera scanner with a dual quasar gradient system with maximum gradient amplitude of 80 mT/m and an eight channel SENSE-compatible head coil (Philips Medical Systems, Best, Netherlands).

2.2.1 Conventional MRI—The MRI protocol included a whole brain high resolution axial 3D T1-weighted volume (voxel size = 0.9375 mm × 0.9375 mm × 0.9375 mm) for automatic brain atlas-based volumetry [31, 32]. In addition, dual fast spin-echo (FSE) images were acquired with echo (T_E) and repetition times of (T_R) of $T_{E1}/T_{E2}/T_R$ = 8.2/90/6800 msec to compute the proton density (PD) and T_2 relaxation time (T_2). A FLAIR sequence with ($T_E/T_I/T_R$ = 80/2500/8000 msec) was used for lesion localization. The slice thickness for both FSE and FLAIR data was 3.0 mm with 44 contiguous axial slices covering the same inferior-to-superior prescription of the 3D T1-weighted sequence and a square field-of-view (FOV) of 240 mm × 240 mm.

2.2.2 Diffusion Tensor Imaging Data Acquisition—DTI data were acquired using a single-shot spin-echo diffusion sensitized echo-planar imaging sequence with balanced Icosa21 tensor encoding scheme with twenty-one uniformly-distributed orientations over the unit hemisphere at b-factor = 1000 sec mm^{-2}, T_R/T_E = 7100/65 msec. The slice thickness, FOV and spatial coverage matched the FSE and FLAIR.

2.3 Conventional MRI and DTI Data Processing

All MRI data sets were masked using the brain extraction tool [33] to remove non-brain tissues and estimate the intracranial volume (ICV) for each subject [20, 29]. A detailed account of these procedures is described elsewhere [31, 32].

2.3.1 FreeSurfer Anatomical Labels and Regional Volumetry Masks—The 3D T1-weighted volumes were prepared for subsequent processing, segmentation and anatomical labeling using FreeSurfer [25] software (http://surfer.nmr.mgh.harvard.edu/fswiki/FreeSurferWiki). FreeSurfer provided volume masks on ~ 180 regions that included cerebrum, cerebellum, brain stem, and cerebrospinal fluid (CSF). The FreeSurfer anatomical labels and their cortical classification are described elsewhere [34]. Only the cerebral cortical, deep gray matter, deep and lobar white matter structures are presented here [31, 32].

Labeled regional volume masks were always obtained in each subject's native space to allow fusion with all other data sets (e.g. lesion, T_2, PD, FA, mean, axial and radial diffusivity maps). Figure 1 illustrates the majority of deep brain subcortical, cortical gray matter and deep and lobar white matter structures generated by FreeSurfer. To simplify the analyses and reduce the number of comparisons we pooled some structures based on their laterality and proximity. First, all structures were analyzed and visualized without pooling. Second, all right and left structures such as caudate (CN) and putamen (PUT) were volume-weighted and averaged. The corpus callosum (CC) midsagittal subdivisions [37] or anterior (aCC), middle anterior (maCC), middle (mCC), isthmus iCC and splenium (sCC) were volume-averaged. Third, the cortical and lobar subdivisions were averaged to obtain single metrics that characterize the frontal, temporal, parietal, occipital, cingulate and insular cortices and the corresponding WM lobes (e.g. frontal lobe WM). The periventricular white matter (PVw) did not belong to any lobar WM territory and may be referred to along with the CC as deep white matter [32, 33].

2.3.2 T_2 Relaxation Time and Proton Density Estimation—The T_2 relaxation time and proton density (PD) values were estimated from the early (T_{E1}) and late echo (T_{E2}) volumes, according to standard spin-echo procedures assuming a single compartment model [20, 36, 37]. The regional PD values were scaled by the PD values in the left accumbens (Ac) obtained from each subject to normalize data and data scaling variation.

2.3.3 Lesion Load Segmentation using Conventional MRI—Whole brain lesion load was quantified in the RRMS group using the coregistered multi-spectral dual FSE and the FLAIR volumes as described elsewhere [38, 39]. The lesion volumes were saved as binary masks to enable fusion with other multimodal volumes acquired from the same subject.

2.3.4 Lesion Probability Map Estimation—Lesion probability maps (LPM) were obtained as described previously [40, 41]. In brief, the T1-weighted volume for each subject was transformed or spatially normalized into the Montreal Neurological Institute (MNI) space, which is commonly used in statistical parametric mapping and adopted by the International Consortium for Brain Mapping (ICBM). The transformation parameters were carried to the lesion mask for each subject [42]. The transformed masks for all RRMS patients were summed on a voxel-by-voxel basis to estimate the regional frequency or lesion occurrence probability or percentage (number divided by total number of patients × 100%) in a certain voxel. The lesion probability masks were visualized in MRIcroN (http://www.nitrc.org/projects/mricron/) and were fused as described below with all qMRI metric data and their correlations with age, expanded disability status scale (EDSS) score, disease duration (DD) in the RRMS group.

2.4 DTI Data Processing

Diffusion-weighted images were intra-registered to the baseline "b_0" images (without diffusion weighting) to correct for the eddy-current-induced image distortions using the software on the Philips PRIDE workstation (Philips Medical Systems, Best, Netherlands). The results of DTI pipeline included b0, FA, mean or average diffusivity (MD = D_{av}), radial diffusivity (RD) and axial diffusivity (AD) maps.

2.5 Multimodal MRI Data Fusion

All conventional MRI-derived volumes (T_2, PD, lesion masks) and DTI-derived data volumes (FA, mean, axial and radial diffusivities) were coregistered to the T1-weighted volume where the FreeSurfer atlas-based volume labels are available in each subject native space. Lesion masks were used to null out the atlas-based volume results [17]. The last step

assured that all cerebral parenchyma tissue used is normal-appearing and lesion free. The qMRI data corresponding to lesions are not analyzed here and only normal-appearing cerebral parenchymal tissue are included. The T_2, PD, FA mean, axial, and radial diffusivity maps were used to estimate the regional atlas-based and volume-wise estimates. The data on all subjects were saved in the analyze file format for further volume-based statistical analyses and visualization.

2.6 Validation and Data Quality

Conventional and DT-MRI data quality and scanner stability were monitored over the 5 year span of data collection. We collected serial data on RRMS patients and healthy controls to assure reproducibility and monitor age-related changes in qMRI metrics (date not shown). All data outputs were inspected at all processing steps to assure the accuracy of volume estimation, alignment of multi-modal MRI and fusion with lesion maps. Lesions were manually checked by a trained rater. Reproducibility and quality control measures are described elsewhere [20, 31, 32, 43].

2.7 Statistical Analysis

Correlations between age, volume-to-ICV percentage, lesion load, disease duration, PD, T_2 values and DTI-derived metrics were computed using the Pearson correlation coefficient. Age-covaried correlations between EDSS score and all other qMRI variables were computed using the Spearman coefficient. For EDSS covariance with lesion load and age multivariate or generalized linear models was used as described elsewhere [44]. Slopes and rates of change of MRI metrics with age were compared using the r to z-Fisher transform. Comparisons between group means and medians were performed using ANOVA (t-test) and the Mann-Whitney U-test. All group comparison differences, significance, rate of change and correlations with age, EDSS, lesion load were computed volume-wise in native data space and were presented in standard space for visual inspection and fusion with the lesion probability maps. All statistical analyses used MATLAB R12.1 Statistical Toolbox v 3.0 (The Mathworks Inc, Natick, MA).

3. Results

3.1 Population Demographics and Clinical Information

Table 1 compares the demographics and MRI whole brain volumetry on the 54 RRMS patients and 88 healthy controls. There were no significant age differences between healthy men and healthy women (p=0.40), nor between RRMS men and RRMS women (p=0.77). Both men and women matched for age range and mean between the two groups (p=0.17). We had disproportionately more women in the RRMS population than in the healthy group consistent with the reported preponderance of RRMS in females [45]. There were no significant differences in the mean values of EDSS (p=0.72), DD (p=0.08) or lesion load (p=0.78) between men and women in the RRMS groups (**p>0.15**). In RRMS patients EDSS correlated significantly with whole brain lesion load (r=0.372; p=0.006) and DD (r=0.30; p=0.028). Lesion load correlated weakly with DD (r=0.228; p=0.097), but not with age (r=0.182; p=0.187). These cross-sectional correlations are generally consistent with well-documented longitudinal and cross-sectional age-related trends in large MS populations [46].

3.2 Normal-Appearing and Healthy Cerebral Volumetry Comparisons

There were significant differences between ICV, total cerebral cortex GM and lobar WM volumes between men and women in the healthy control ($p < 0.0001$) and RRMS groups ($p < 0.0005$). These gender-based skull size related differences were not significant in the two

groups upon scaling or covarying the volumetry values with the ICV ($p > 0.14$; see Table 1). Therefore, for all subsequent analyses men and women were pooled in each group and all regional volumes were scaled by the each subject's ICV value.

3.3 Regional Quantitative MRI Differences between Healthy Controls and RRMS

Figure 2 summarizes the group mean values and their significance between RRMS patients and controls for the corpus striatum, hippocampus/amygdala, entire CC, periventricular WM, cerebral cortex parcellations and corresponding lobar WM using several qMRI metrics: (A) absolute volume in mL, (B) volume percentage, (C) relative proton density, and (D) T_2 relaxation time. Figure 3 shows (A) fractional anisotropy, (B) mean, (C) axial, and (D) radial diffusivities. The mean values for qMRI metrics in RRMS patients are significantly different from controls. Note that *all* cortical and subcortical structures in the RRMS cerebrum have elevated mean diffusivity compared to the control group (**$p<0.005$**). With the exception of the NAGM in the occipital and cingulate cortices, all cerebral regions are atrophic (e.g. have reduced volume-to-ICV percentage = VOLp). All these structures have elevated T_2 *except* for the corpus striatum which has lower T_2 values in the RRMS group. Note that both FA and VOLp did not exhibit the widespread sensitivity to injury mechanisms in RRMS as captured by the T_2, mean, radial or axial diffusivity average values.

3.4 Age correlations with regional qMRI values in RRMS and Healthy Controls

It is well-documented that whole brain gray matter [29, 37, 47, 48], cortical [47] and subcortical [20, 30, 37, 49] undergo age-related volume loss. Therefore, it is important to attempt to decouple natural age-related changes from MS pathology effects [20, 30]. As an illustration of these age effects and demonstration of data quality, Figure 4 shows representative scatter plots of the total frontal (Fig. 4a) and cingulate (Fig. 4b) cortices VOLp and their corresponding mean diffusivity. Note the rapid decrease of VOLp with age in both MS and controls (atrophy rate or slopes did not differ $p > 0.2$). The mean diffusivity average value in the frontal (Fig. 4c) and cingulate (Fig. 4d) cortices while significantly higher in RRMS ($p < 1 \times 10^{-9}$) also increased with age more rapidly in RRMS compared to controls ($p < 1 \times 10^{-13}$). Note that while the total VOLp of the NAGM of the cingulate cortex is not different in RRMS compared to controls ($p=0.30$; Fig. 4a see also Fig. 2 and Fig. 3), the mean diffusivity of the cingulate cortex (Fig. 4d) is greater in RRMS ($p = 3.2 \times 10^{-10}$). Moreover, the difference between RRMS and controls in mean diffusivity seems to increase with age due to increasing disease duration..

3.5 Visualization of Lesions and Regional qMRI Differences between Controls and RRMS

Figure 5 illustrates the interplay between spatial locations of lesions and regional volume-averaged qMRI metrics of normal-appearing WM and GM. The figure fuses lesion occurrence probability with the percentage difference in VOLp between controls and RRMS. The percentage VOLp difference between RRMS and controls was largest in the periventricular white matter and the isthmus of the corpus callosum. Lesions were most frequent in the periventricular and occipital lobe WM where the atrophy is greatest. Lesions were least frequent in the putamen, thalamus proper and amygdalae.

3.6 Age-covaried regional qMRI in normal-appearing Tissue with Clinical Scores in RRMS

The age-adjusted regional correlations and corresponding significance of all qMRI metrics in normal-appearing tissue with the global lesion load and disease duration are summarized in Table 2 and Table 3, respectively. Table 4 provides the correlations of normal-appearing qMRI metrics with EDSS adjusting for both age and total lesion load. This analysis was done to attempt to decouple the contributions from both natural aging and the cumulative or

residual effects of MRI-defined lesions on the regional qMRI metrics or normal-appearing tissue. Note that a few lobar, periventricular and deep WM structures such as corpus callosum remained significant ($p \leq 0.05$; not accounting for multiple comparisons) and in particular the axial diffusivity. Note that regional white matter metrics (e.g. CC) provide more significant correlations than global metrics.

4. Discussion

This is likely the first comprehensive report relaxation time, proton density, diffusion anisotropy, mean, axial and radial diffusivity measurements of the cerebral subcortical and cortical white and gray matter subdivisions in relatively large cohorts of controls and RRMS patients. We have presented both global and regional macrostructural and atrophy measures in addition to microstructural attributes of normal-appearing tissue using volume-based methods. We have fused FreeSurfer volumetry with lesion maps, proton density, T_2 relaxation, and DTI-derived volumes in each subject's native space.

In this work, the mean diffusivity and relaxation time have been shown to be quite abnormal in MS whereas regional tissue volume was only slightly reduced. The dissociation between macrostructual metrics and microstructural attributes has been reported in development and natural aging and MS [20]. Consistent with a previous report in MS [50], we also found that FA was a less sensitive measure than mean diffusivity. This particular finding is not surprising as FA is a ratio measure of two variables (axial and radial diffusivities) that could be affected equally by factors such as edema which would have increased both axial and radial diffusivities [51].

4.1 Consistency of findings with literature in MS

Our findings of abnormal and widespread injury in MS are consistent with previous histopathological [2, 52, 53, 54] and *in vivo* hypoperfusion [16, 55, 56, 57] and reduced glucose metabolism [55, 58, 59] when investigating MS patients with different stages or with different phenotypes. Our observations of significant tissue volume loss in MS patients are consistent with previous report [12] using voxel-based [18, 19], tract-based [17], volume-based methods [20, 21]. These studies collectively showed atrophic corpus callosum [59], hippocampus [60], caudate [20, 28, 30, 61], putamen [19, 21, 28], thalamus [19, 21, 28], and cortical GM [27, 28].

The present findings of reduced T_2 in normal-appearing deep corpus striatum structures such as caudate and putamen are consistent with previous intensity-based [6], quantitative relaxometry reports [20], and iron mapping methods [62, 63]. Our finding of decreased T_2 in the caudate and putamen supports the accuracy of the processing procedures adopted in this study as any contamination with neighboring CSF would have elevated basal ganglia T_2 values due to CSF ventricular expansion in MS patients. The widespread elevation in T_2 values in cortical GM, deep and lobar white matter confirms previous [64] and recent reports [36].

The widespread and significant increase in mean, axial and radial diffusivities in deep and cortical gray and lobar white matter is consistent with several reports [12, 65]. The elevated diffusivity in MS normal-appearing tissue such as corpus callosum [66], hippocampus [67], thalamus [68, 69], and compact WM fiber tracks [17, 70] may be attributed to demyelination and axonal injury [2].

Our qMRI findings of widespread injury in RRMS are also in line with previous reports using different MRI approaches [12] that include volumetry (e.g. anatomical length or distance, area, thickness) [27], T1-relaxation time [71, 72], magnetization transfer ratio [12],

myelin water fraction [73], MR spectroscopy [56, 66], functional MRI [74], perfusion [16, 75], brain tissue sodium concentration [76], and cerebral MR elastography [77],

4.2 Lesion Distribution and Clinical Correlations

The spatial distribution of lesions on our RRMS cohort is similar to previous reports [40, 41, 78, 79] in which lesions were shown to most frequent in periventricular white matter as has also been reported *postmortem* [80]. The lesion frequency in our RRMS cohort was least frequent in the putamen and thalamus as has been also reported in previous imaging [57, 59, 68] and postmortem reports [80]. The predilection or vulnerability of deep white matter to lesion formation and relative sparing of deep gray matter from lesion formation has been attributed by Brownell and Hughes [80] to vascular perfusion which is highest in normal adult deep GM compared to white matter [4, 75, 82]. A detailed analysis of the qMRI correlates of lesion distribution is beyond the scope of this work, but will be the subject of future endeavors.

4.3 Correlations of of RRMS Disability Scores and qMRI Correlations

An important finding of this work is the elevated normal-appearing cortical mean diffusivity which correlated strongly with EDSS adjusted for age and whole brain lesion load. Cortical volumetry did not show this relationship, likely because these structures also undergo age-related changes [47]. Decoupling age-related degeneration is important to separate the confounding effect of natural aging on the lesion-driven pathology. The frontal, parietal, cingulate, insular lobes, corpus callosum, and periventricular white matter zones showed significant correlation with EDSS adjusted for age and lesion load. The EDSS correlation of the periventricular WM with transverse diffusivity did not reach significance ($p=0.07$), but this may indicate that demyelination as indexed by radial diffusivity in this lesion-dense zone may be operative and contributing to connected tissue loss.

Another important finding in this work is that the corpus callosum volume reduction, callosal elevation in T_2, increased mean and axial diffusivities was decoupled from lesion load and age-related degeneration. The observation in RRMS that the axial diffusivity is elevated in the atrophic corpora callosa (Fig. 2, Fig. 3) and that the age and lesion load adjusted axial diffusivity in callosal subregions (Table 4) was significantly correlated with EDSS indicates that this metric is sensitive to chronic axonal injury or degeneration as has been reported on the CC using combined spectroscopy [66] and DTI tractography studies [17, 70], histopathology [52] and using animal models of tissue injury [82, 83, 84].

5. Limitations, Conclusions and Future Plans

Using standardized multimodal qMRI data and analyses that accounted for lesion distribution and natural aging we were able to demonstrate that pathology is widespread over the cerebrum in RRMS. Moreover, we were able to identify *in vivo* MRI markers of demyelination and axonal injury in white matter.. Limitations of this work include the inherent limitations MRI to small lesions that could not be detected with our protocol and the need for larger populations with serial data to test the cross-sectional findings further. Nevertheless, our study included a large healthy adult control population and we accounted for the confounding effects of natural aging. Our approach warrants further application to serial data and the extension to other MS phenotypes.

Acknowledgments

This work is funded by the National institutes of Health (NIH/NINDS R01-NS052505-04 and Dunn Research Foundation to KMH, NIH/NIBIB EB002095 to PAN, and an unrestricted gift from the Band Against Multiple

Sclerosis to JSW. The purchase of the 3.0 T MRI Clinical Scanner is partially funded by NIH grant S10 RR19186 to PAN. We wish to thank Vipul Kumar Patel for helping in data acquisition.

References

[1]. Barnett MH, Prineas JW. Relapsing and remitting multiple sclerosis: pathology of the newly forming lesion. Ann Neurol. 2004; 55:458–68. [PubMed: 15048884]

[2]. Seewann A, Vrenken H, van der Valk P, Blezer EL, Knol DL, Castelijns JA, et al. Diffusely abnormal white matter in chronic multiple sclerosis: imaging and histopathologic analysis. Arch Neurol. 2009; 66:601–9. [PubMed: 19433660]

[3]. Trapp BD, Peterson J, Ransohoff RM, Rudick R, Mork S, Bo L. Axonal transection in the lesions of multiple sclerosis. New Engl J Med. 1998; 338:278–85. [PubMed: 9445407]

[4]. D'haeseleer M, Cambron M, Vanopdenbosch L, De Keyser J. Vascular aspects of multiple sclerosis. Lancet Neurol. 2011; 10:657–66. [PubMed: 21683931]

[5]. Pozzilli C, Bernardi S, Mansi L, Picozzi P, Iannotti F, Alfano B, et al. Quantitative assessment of blood-brain barrier permeability in multiple sclerosis using 68-Ga-EDTA and positron emission tomography. J Neurol Neurosurg Psychiatry. 1988; 51:1058–62. [PubMed: 3145963]

[6]. Brass SD, Chen NK, Mulkern RV, Bakshi R. Magnetic resonance imaging of iron deposition in neurological disorders. Top Magn Reson Imaging. 2006; 17:31–40. Review. [PubMed: 17179895]

[7]. Dutta R, McDonough J, Yin X, Peterson J, Chang A, Torres T, et al. Mitochondrial dysfunction as a cause of axonal degeneration in multiple sclerosis patients. Ann. Neurol. 2006; 59:478–489. [PubMed: 16392116]

[8]. Waxman SG. Axonal conduction and injury in multiple sclerosis: the role of sodium channels. Nat Rev Neurosci. 2006; 7:932–41. Review. [PubMed: 17115075]

[9]. Lassmann H. Multiple sclerosis: is there neurodegeneration independent from inflammation? J Neurol Sci. 2007; 259:3–6. [PubMed: 17367814]

[10]. Young IR, Hall AS, Pallis CA, Legg NJ, Bydder GM, Steiner RE. Nuclear magnetic resonance imaging of the brain in multiple sclerosis. Lancet. 1981; 2:1063–6. [PubMed: 6118521]

[11]. Goodin DS. Magnetic resonance imaging as a surrogate outcome measure of disability in multiple sclerosis: have we been overly harsh in our assessment? Ann Neurol. 2006; 59:597–605. Review. [PubMed: 16566022]

[12]. Filippi M, Agosta F. Imaging biomarkers in multiple sclerosis. J Magn Reson Imaging. 2010; 31:770–88. Review. [PubMed: 20373420]

[13]. Barkhof F. The clinico-radiological paradox in multiple sclerosis revisited. Curr Opin Neurol. 2002; 15:239–45. Review. [PubMed: 12045719]

[14]. Ciccarelli O, Werring DJ, Wheeler-Kingshott CA, Barker GJ, Parker GJ, Thompson AJ, et al. Investigation of MS normal-appearing brain using diffusion tensor MRI with clinical correlations. Neurology. 2001; 56:926–33. [PubMed: 11294931]

[15]. Hasan KM, Gupta RK, Santos RM, Wolinsky JS, Narayana PA. Diffusion tensor fractional anisotropy of the normal-appearing seven segments of the corpus callosum in healthy adults and relapsing-remitting multiple sclerosis patients. J Magn Reson Imaging. 2005; 21:735–43. [PubMed: 15906348]

[16]. Law M, Saindane AM, Ge Y, Babb JS, Johnson G, Mannon LJ, Herbert J, Grossman RI. Microvascular abnormality in relapsing-remitting multiple sclerosis: perfusion MR imaging findings in normal-appearing white matter. Radiology. 2004; 231:645–52. [PubMed: 15163806]

[17]. Rocca MA, Pagani E, Absinta M, Valsasina P, Falini A, Scotti G, et al. Altered functional and structural connectivities in patients with MS: a 3-T study. Neurology. 2007; 69:2136–45. [PubMed: 18056577]

[18]. Roosendaal SD, Geurts JJ, Vrenken H, Hulst HE, Cover KS, Castelijns JA, et al. Regional DTI differences in multiple sclerosis patients. Neuroimage. 2009; 44:1397–403. [PubMed: 19027076]

[19]. Tao G, Datta S, He R, Nelson F, Wolinsky JS, Narayana PA. Deep gray matter atrophy in multiple sclerosis: a tensor based morphometry. J Neurol Sci. 2009; 282:39–46. [PubMed: 19168189]

[20]. Hasan KM, Halphen C, Kamali A, Nelson FM, Wolinsky JS, Narayana PA. Caudate nuclei volume, diffusion tensor metrics, and T(2) relaxation in healthy adults and relapsing-remitting multiple sclerosis patients: implications for understanding gray matter degeneration. J Magn Reson Imaging. 2009; 29:70–7. [PubMed: 19097116]

[21]. Ramasamy DP, Benedict RH, Cox JL, Fritz D, Abdelrahman N, Hussein S, et al. Extent of cerebellum, subcortical and cortical atrophy in patients with MS: a case-control study. J Neurol Sci. 2009; 282:47–54. [PubMed: 19201003]

[22]. De Stefano N, Narayanan S, Francis SJ, Smith S, Mortilla M, Tartaglia MC, et al. Diffuse axonal and tissue injury in patients with multiple sclerosis with low cerebral lesion load and no disability. Arch Neurol. 2002; 59:1565–71. [PubMed: 12374493]

[23]. Filippi M, Rocca MA. MRI evidence for multiple sclerosis as a diffuse disease of the central nervous system. J Neurol. 2005; 252:v16–24. Review. [PubMed: 16254697]

[24]. Chard D, Miller D. Is multiple sclerosis a generalized disease of the central nervous system? An MRI perspective. Curr Opin Neurol. 2009; 22:214–8. Review. [PubMed: 19434770]

[25]. Fischl B, Salat DH, Busa E, Albert M, Dieterich M, Haselgrove C, et al. Whole brain segmentation: automated labeling of neuroanatomical structures in the human brain. Neuron. 2002; 33:341–55. [PubMed: 11832223]

[26]. Derakhshan M, Caramanos Z, Giacomini PS, Narayanan S, Maranzano J, Francis SJ, Arnold DL, Collins DL. Evaluation of automated techniques for the quantification of grey matter atrophy in patients with multiple sclerosis. Neuroimage. 2010; 52:1261–67. [PubMed: 20483380]

[27]. Sailer M, Fischl B, Salat D, Tempelmann C, Schönfeld MA, Busa E, et al. Focal thinning of the cerebral cortex in multiple sclerosis. Brain. 2003; 126:1734–44. [PubMed: 12805100]

[28]. Pellicano C, Gallo A, Li X, Ikonomidou VN, Evangelou IE, Ohayon JM, et al. Relationship of cortical atrophy to fatigue in patients with multiple sclerosis. Arch Neurol. 2010; 67:447–53. [PubMed: 20385911]

[29]. Courchesne E, Chisum HJ, Townsend J, Cowles A, Covington J, Egaas B, Harwood M, Hinds S, Press GA. Normal brain development and aging: quantitative analysis at in vivo MR imaging in healthy volunteers. Radiology. 2000; 216:672–82. [PubMed: 10966694]

[30]. Kassubek J, Tumani H, Ecker D, Kurt A, Ludolph AC, Juengling FD. Age-related brain parenchymal fraction is significantly decreased in young multiple sclerosis patients: a quantitative MRI study. Neuroreport. 2003; 14:427–30. [PubMed: 12634497]

[31]. Walimuni IS, Hasan KM. Atlas-based investigation of human brain tissue microstructural spatial heterogeneity and interplay between transverse relaxation time and radial diffusivity. Neuroimage. 2011; 57:1402–10. [PubMed: 21658457]

[32]. Hasan KM, Walimuni IS, Kramer LA, Narayana PA. Human brain iron mapping using atlas-based T(2) relaxometry. Magn Reson Med. 2011 doi: 10.1002/mrm.23054.

[33]. Smith SM. Fast robust automated brain extraction. Human Brain Mapping. 2002; 17:143–55. [PubMed: 12391568]

[34]. Desikan RS, Ségonne F, Fischl B, Quinn BT, Dickerson BC, Blacker D, et al. An automated labeling system for subdividing the human cerebral cortex on MRI scans into gyral based regions of interest. Neuroimage. 2006; 31:968–80. [PubMed: 16530430]

[35]. Witelson SF. Hand and sex differences in the isthmus and genu of the human corpus callosum. A postmortem morphological study. Brain. 1989; 112:799–835. [PubMed: 2731030]

[36]. Neema M, Goldberg-Zimring D, Guss ZD, Healy BC, Guttmann CR, Houtchens MK, et al. 3 T MRI relaxometry detects T2 prolongation in the cerebral normal-appearing white matter in multiple sclerosis. Neuroimage. 2009; 46:633–41. [PubMed: 19281850]

[37]. Hasan KM, Walimuni IS, Kramer LA, Frye RE. Human brain atlas-based volumetry and relaxometry: application to healthy development and natural aging. Magn Reson Med. 2010; 64:1382–89. [PubMed: 20740662]

[38]. Sajja BR, Datta S, He R, Mehta M, Gupta RK, Wolinsky JS, Narayana PA. Unified approach for multiple sclerosis lesion segmentation on brain MRI. Ann Biomed Eng. 2006; 34:142–51. [PubMed: 16525763]

[39]. Datta S, Sajja BR, He R, Wolinsky JS, Gupta RK, Narayana PA. Segmentation and quantification of black holes in multiple sclerosis. NeuroImage. 2006; 29:467–74. [PubMed: 16126416]

[40]. Narayanan S, Fu L, Pioro E, De Stafano N, Collins DL, Francis GS, et al. Imaging of axonal damage in multiple sclerosis: spatial distribution of magnetic resonance imaging lesions. Ann Neurol. 1997; 41:385–91. [PubMed: 9066360]

[41]. Zijdenbos AP, Forghani R, Evans AC. Automatic “pipeline” analysis of 3-D MRI data for clinical trials: application to multiple sclerosis. IEEE Trans Med Imaging. 2002; 21:1280–91. [PubMed: 12585710]

[42]. Brett M, Leff AP, Rorden C, Ashburner J. Spatial normalization of brain images with focal lesions using cost function masking. Neuroimage. 2001; 14:486–500. [PubMed: 11467921]

[43]. Hasan KM. A framework for quality control and parameter optimization in diffusion tensor imaging: theoretical analysis and validation. Magn Reson Imaging. 2007; 25:1196–202. [PubMed: 17442523]

[44]. Fu L, Wolfson C, Worsley KJ, De Stefano N, Collins DL, Narayanan S, et al. Statistics for investigation of multimodal MR imaging data and an application to multiple sclerosis patients. NMR Biomed. 1996; 9:339–46. [PubMed: 9176888]

[45]. Achiron A, Gurevich M. Gender effects in relapsing-remitting multiple sclerosis: correlation between clinical variables and gene expression molecular pathways. J Neurol Sci. 2009; 286:47–53. [PubMed: 19596127]

[46]. Trojano M, Liguori M, Bosco Zimatore G, Bugarini R, Avolio C, Paolicelli D, Giuliani F, De Robertis F, Marrosu MG, Livrea P. Age-related disability in multiple sclerosis. Ann Neurol. 2002; 51:475–80. [PubMed: 11921053]

[47]. Sowell ER, Peterson BS, Thompson PM, Welcome SE, Henkenius AL, Toga AW. Mapping cortical change across the human life span. Nat Neurosci. 2003; 6:309–15. [PubMed: 12548289]

[48]. Hasan KM, Sankar A, Halphen C, Kramer LA, Brandt ME, Juranek J, et al. Development and organization of the human brain tissue compartments across the lifespan using diffusion tensor imaging. Neuroreport. 2007; 18:1735–9. [PubMed: 17921878]

[49]. Hasan KM, Frye RE. Diffusion tensor-based regional gray matter tissue segmentation using the international consortium for brain mapping atlases. Hum Brain Mapp. 2011; 32:107–17. [PubMed: 20799340]

[50]. Castriota-Scanderbeg A, Fasano F, Hagberg G, Nocentini U, Filippi M, Caltagirone C. Coefficient (Dav) is more sensitive than fractional anisotropy in monitoring progression of irreversible tissue damage in focal nonactive multiple sclerosis lesions. AJNR Am J Neuroradiol. 2003; 24:663–70. [PubMed: 12695200]

[51]. Mukherjee P, Miller JH, Shimony JS, Conturo TE, Lee BC, Almli CR, et al. Diffusion-tensor MR imaging of gray and white matter development during 21 normal human brain maturation. AJNR Am J Neuroradiol. 2002; 23:1445–56. [PubMed: 12372731]

[52]. Evangelou N, Esiri MM, Smith S, Palace J, Matthews PM. Quantitative pathological evidence for axonal loss in normal appearing white matter in multiple sclerosis. Ann Neurol. 2000; 47:391–5. [PubMed: 10716264]

[53]. Cifelli A, Arridge M, Jezzard P, Esiri MM, Palace J, Matthews PM. Thalamic neurodegeneration in multiple sclerosis. Ann Neurol. 2002; 52:650–3. [PubMed: 12402265]

[54]. Geurts JJ, Bö L, Roosendaal SD, Hazes T, Daniëls R, Barkhof F, Witter MP, Huitinga I, van der Valk P. Extensive hippocampal demyelination in multiple sclerosis. J Neuropathol Exp Neurol. 2007; 66:819–27. [PubMed: 17805012]

[55]. Brooks DJ, Leenders KL, Head G, Marshall J, Legg NJ, Jones T. Studies on regional cerebral oxygen utilisation and cognitive function in multiple sclerosis. J Neurol Neurosurg Psychiatry. 1984; 47:1182–91. [PubMed: 6334132]

[56]. Schiepers C, Van Hecke P, Vandenberghe R, Van Oostende S, Dupont P, Demaerel P, et al. Positron emission tomography, magnetic resonance imaging and proton NMR spectroscopy of white matter in multiple sclerosis. Mult Scler. 1997; 3:8–17. [PubMed: 9160342]

[57]. Derache N, Marie RM, Constans JM, Defer GL. Reduced thalamic and cerebellar rest metabolism in relapsing-remitting multiple sclerosis, a positron emission tomography study: correlations to lesion load. J Neurol Sci. 2006; 245:103–109. [PubMed: 16647086]

[58]. Pozzilli C, Fieschi C, Perani D, Paulesu E, Comi G, Bastianello S, et al. Relationship between corpus callosum atrophy and cerebral metabolic asymmetries in multiple sclerosis. J Neurol Sci. 1992; 112:51–7. [PubMed: 1469440]

[59]. Blinkenberg M, Rune K, Jensen CV, Ravnborg M, Kyllingsbaek S, Holm S, et al. Cortical cerebral metabolism correlates with MRI lesion load and cognitive dysfunction in MS. Neurology. 2000; 54:558–64. [PubMed: 10680783]

[60]. Sicotte NL, Kern KC, Giesser BS, Arshanapalli A, Schultz A, Montag M, et al. Regional hippocampal atrophy in multiple sclerosis. Brain. 2008; 131:1134–41. [PubMed: 18375977]

[61]. Bermel RA, Innus MD, Tjoa CW, Bakshi R. Selective caudate atrophy in multiple sclerosis: a 3D MRI parcellation study. Neuroreport. 2003; 14:335–9. [PubMed: 12634479]

[62]. MacKay AL, Vavasour IM, Rauscher A, Kolind SH, Mädler B, Moore GR, Traboulsee AL, Li DK, Laule C. MR relaxation in multiple sclerosis. Neuroimaging Clin N Am. 2009; 19(1):1–26. Review. [PubMed: 19064196]

[63]. Ge Y, Jensen JH, Lu H, Helpern JA, Miles L, Inglese M, et al. Quantitative assessment of iron accumulation in the deep gray matter of multiple sclerosis by magnetic field correlation imaging. AJNR Am J Neuroradiol. 2007; 28:1639–44. [PubMed: 17893225]

[64]. Larsson HB, Thomsen C, Frederiksen J, Stubgaard M, Henriksen O. In vivo magnetic resonance diffusion measurement in the brain of patients with multiple sclerosis. Magn Reson Imaging. 1992; 10:7–12. [PubMed: 1545684]

[65]. Inglese M, Bester M. Diffusion imaging in multiple sclerosis: research and clinical implications. NMR Biomed. 2010; 23:865–72. [PubMed: 20882528]

[66]. Cader S, Johansen-Berg H, Wylezinska M, Palace J, Behrens TE, Smith S, et al. Discordant white matter N-acetylasparate and diffusion MRI measures suggest that chronic metabolic dfunction contributes to axonal pathology in multiple sclerosis. NeuroImage. 2007; 36:19–27. [PubMed: 17398118]

[67]. Vrenken H, Pouwels PJ, Geurts JJ, Knol DL, Polman CH, Barkhof F, et al. Altered diffusion tensor in multiple sclerosis normal-appearing brain tissue: cortical diffusion changes seem related to clinical deterioration. J Magn Reson Imaging. 2006; 23:628–36. [PubMed: 16565955]

[68]. Tovar-Moll F, Evangelou IE, Chiu AW, Richert ND, Ostuni JL, Ohayon JM, et al. Thalamic involvement and its impact on clinical disability in patients with multiple sclerosis: a diffusion tensor imaging study at 3T. AJNR Am J Neuroradiol. 2009; 30:1380–6. [PubMed: 19369608]

[69]. Henry RG, Shieh M, Amirbekian B, Chung S, Okuda DT, Pelletier D. Connecting white matter injury and thalamic atrophy in clinically isolated syndromes. J Neurol Sci. 2009; 282:61–6. [PubMed: 19394969]

[70]. Fink F, Klein J, Lanz M, Mitrovics T, Lentschig M, Hahn HK, et al. Comparison of diffusion tensor-based tractography and quantified brain atrophy for analyzing demyelination and axonal loss in MS. J Neuroimaging. 2010; 20:334–44. [PubMed: 19453832]

[71]. Parry A, Clare S, Jenkinson M, Smith S, Palace J, Matthews PM. MRI brain T1 relaxation time changes in MS patients increase over time in both the white matter and the cortex. J Neuroimaging. 2003; 13:234–9. [PubMed: 12889170]

[72]. Niepel G, Tench ChR, Morgan PS, Evangelou N, Auer DP, Constantinescu CS. Deep gray matter and fatigue in MS: a T1 relaxation time study. J Neurol. 2006; 253:896–902. [PubMed: 16525881]

[73]. Laule C, Vavasour IM, Moore GR, Oger J, Li DK, Paty DW, et al. Water content and myelin water fraction in multiple sclerosis. A T2 relaxation study. J Neurol. 2004; 251:284–93. [PubMed: 15015007]

[74]. Lowe MJ, Phillips MD, Lurito JT, Mattson D, Dzemidzic M, Mathews VP. Multiple sclerosis: low-frequency temporal blood oxygen level-dependent fluctuations indicate reduced functional connectivity initial results. Radiology. 2002; 224:184–92. [PubMed: 12091681]

[75]. Varga AW, Johnson G, Babb JS, Herbert J, Grossman RI, Inglese M. White matter hemodynamic abnormalities precede sub-cortical gray matter changes in multiple sclerosis. J Neurol Sci. 2009; 282:28–33. [PubMed: 19181347]

[76]. Inglese M, Madelin G, Oesingmann N, Babb JS, Wu W, Stoeckel B, et al. Brain tissue sodium concentration in multiple sclerosis: a sodium imaging study at 3 tesla. Brain. 2010; 133:847–57. [PubMed: 20110245]

[77]. Wuerfel J, Paul F, Beierbach B, Hamhaber U, Klatt D, Papazoglou S. MR-elastography reveals degradation of tissue integrity in multiple sclerosis. Neuroimage. 2010; 49:2520–5. [PubMed: 19539039]

[78]. Vellinga MM, Geurts JJ, Rostrup E, Uitdehaag BM, Polman CH, Barkhof F, Vrenken H. Clinical correlations of brain lesion distribution in multiple sclerosis. J Magn Reson Imaging. 2009; 29:768–73. [PubMed: 19306365]

[79]. Ceccarelli A, Rocca MA, Pagani E, Colombo B, Martinelli V, Comi G, et al. A voxel-based morphometry study of grey matter loss in MS patients with different clinical phenotypes. Neuroimage. 2008; 42:315–22. [PubMed: 18501636]

[80]. Brownell B, Hughes JT. The distribution of plaques in the cerebrum in multiple sclerosis. J Neurol Neurosurg Psychiatry. 1962; 25:315–20. [PubMed: 14016083]

[81]. Ito H, Kanno I, Takahashi K, Ibaraki M, Miura S. Regional distribution of human cerebral vascular mean transit time measured by positron emission tomography. Neuroimage. 2003; 19:1163–9. [PubMed: 12880841]

[82]. Kinoshita Y, Ohnishi A, Kohshi K, Yokota A. Apparent diffusion coefficient on rat brain and nerves intoxicated with methylmercury. Environ Res. 1999; 80:348–54. [PubMed: 10330308]

[83]. Song SK, Yoshino J, Le TQ, Lin SJ, Sun SW, Cross AH, Armstrong RC. Demyelination increases radial diffusivity in corpus callosum of mouse brain. Neuroimage. 2005; 15(26):132–40. [PubMed: 15862213]

[84]. Beaulieu C. The basis of anisotropic water diffusion in the nervous system - a technical review. NMR Biomed. 2002; 15:435–55. Review. [PubMed: 12489094]

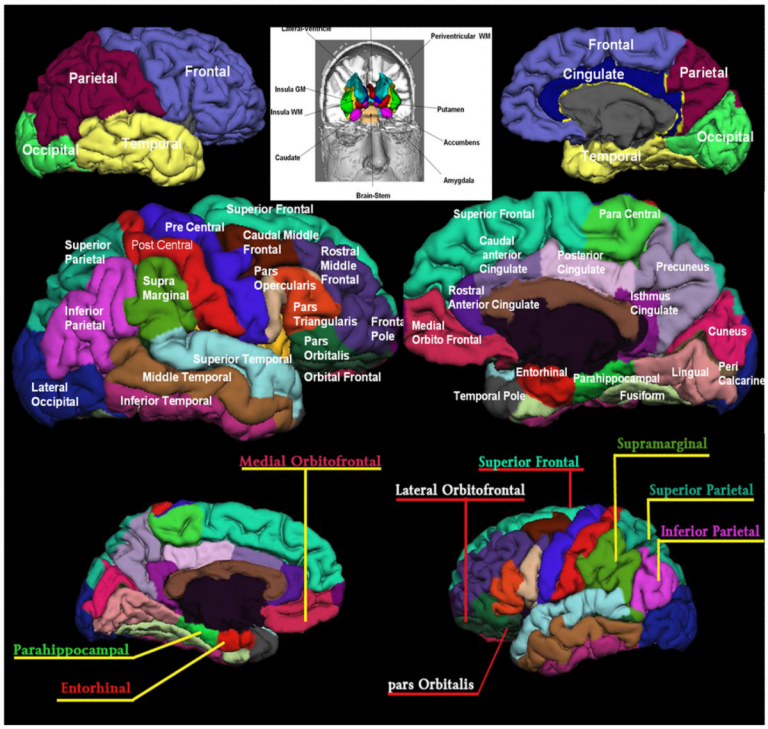

Figure 1.

Illustration of the FreeSurfer generated deep and cortical brain regions. The cortical (e.g. frontal cortex subdivisions) or deep (e.g. corpus callosum subdivisions) were pooled or volume-averaged as needed to reduce the number of comparisons.

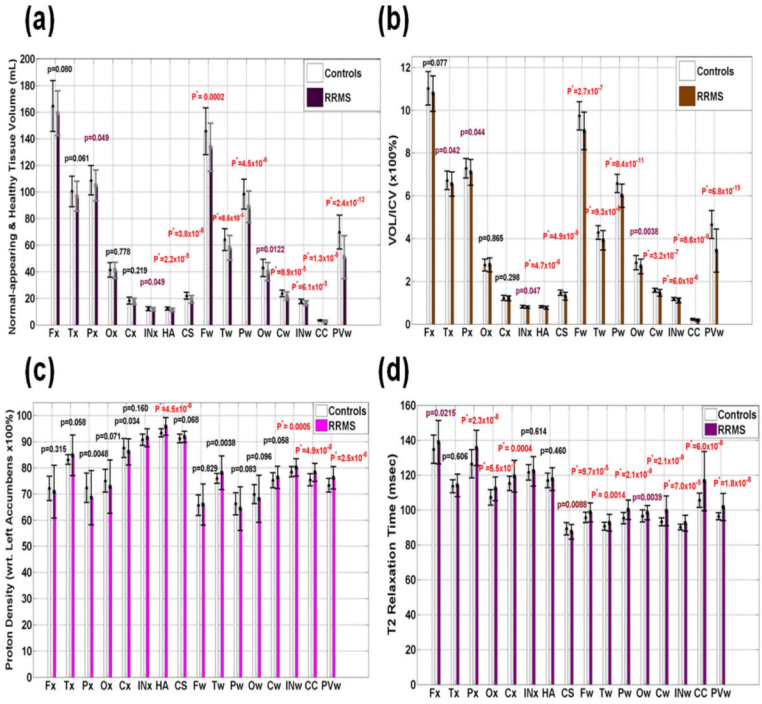

Figure 2.

Group mean comparisons of regional normal-appearing qMRI values between controls and RRMS (subcortical, cortical and lobar white and gray matter) (a) absolute volume in mL, (b) volume-to-ICV percentage or VOLp (c) relative proton density, and (d) T_2 relaxation time

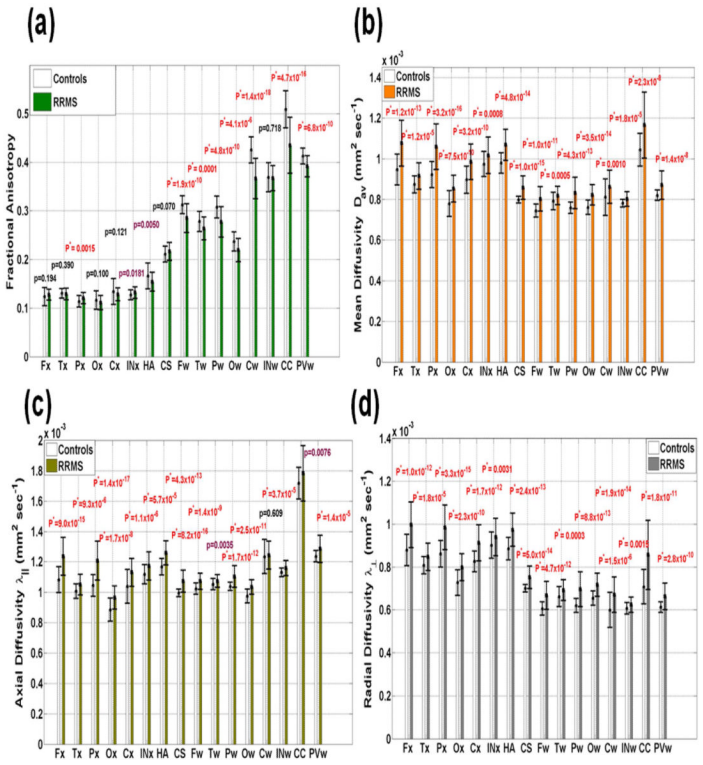

Figure 3.

Group mean comparisons of regional normal-appearing qMRI values between controls and RRMS (subcortical, cortical and lobar white and gray matter) (a) fractional anisotropy, (b) mean diffusivity, (c) axial diffusivity, and (d) radial diffusivity.

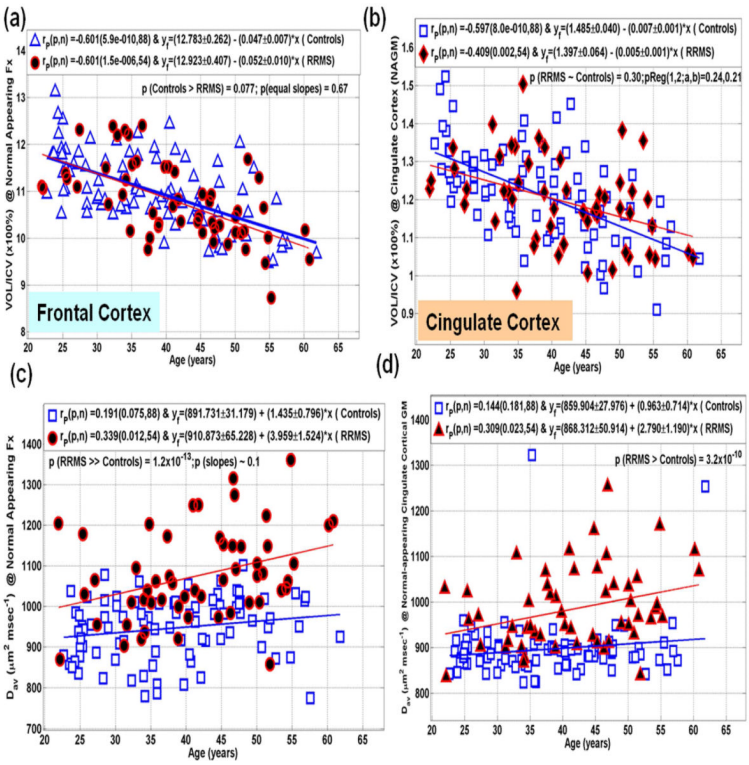

Figure 4.

Representative illustration of age-dependence of qMRI metrics in both RRMS and controls using scatter plots and linear regression (a) volume percentage of the frontal cortex (b) volume percentage of the cingulate cortex (c) mean diffusivity of the frontal cortex and (d) mean diffusivity of the cingulate cortex. Note the rapid decrease in cortical gray matter volume with age in both controls and RRMS patients.

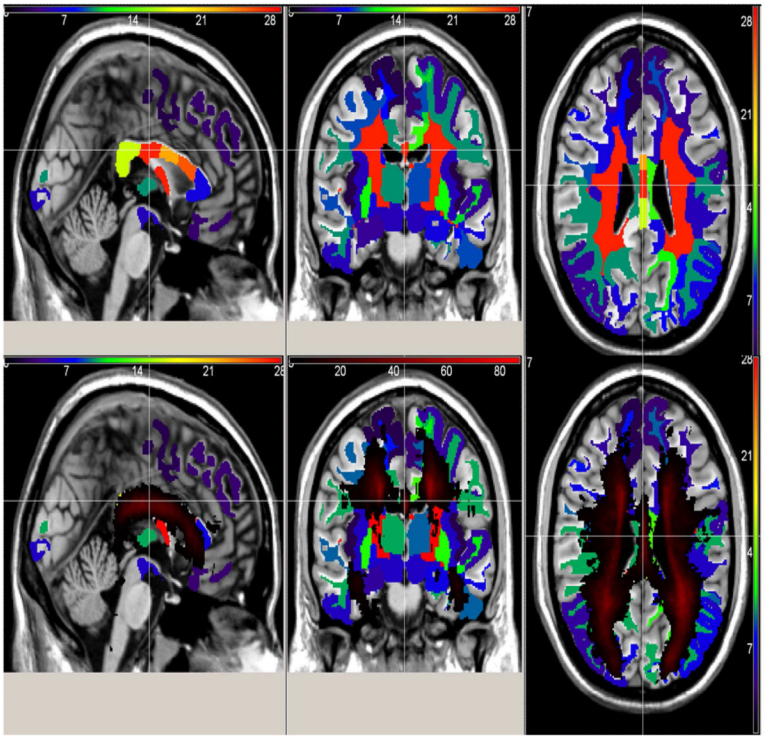

Figure 5.

Visual illustration of regional qMRI and fusion with lesion probability maps in RRMS. The upper multi-plane view shows the percentage ICV-normalized normal-appearing volume difference (significant atrophy RRMS < Controls) fused with the lesion map (lower multi-view). Note that largest normal-appearing tissue atrophy is in deep white matter where lesion probability map is largest. Note that lesions in our RRMS cohort were least frequent in the thalamus yet the volume difference is significant. The color map (minimum dark blow) in the upper views corresponds to the percentage (maximum ~ 28% (bright red) in periventricular white matter and corpus callosum isthmus; see Fig 2b for the corresponding group difference p values. The color map in the middle lower view corresponds to the percentage of patients with lesions.

Table 1

Main demographic, clinical and MRI derived characteristics of the healthy RRMS patients and healthy controls. The MRI derived metrics include the intracranial volume (ICV), normal-appearing cortical gray matter (NACGM), normal-appearing lobar white matter NALWM and lateral ventricular CSF volume –to-ICV percentage.

	RRMS Patients	**Healthy Controls**	**% Difference (RRMS-HC)/ HC (x100)**	**P value**
Number	54	88		
F:M (F/M Ratio)	39:15 (2.6)	47:41 (1.15)		**0.0004**
Age (years)	41.7 ± 9.6 [22.0-60.8]	37.9 ± 10.0 [22.7-61.8]	**10.1**	**0.03**
Disease Duration (years)	9.3 ± 8.7 [0.2-35.4]	N. A	N. A	N. A
EDSS	1.6 ± 1.5 [0.0-6.5]	N. A	N. A	N. A
T2 LL (mL)	13.2 ± 12.3 [0.2-44.8]	N. A	N. A	N. A
Icv	1478.1 ± 132.6 [1196.3 - 1921.4]	1494.2 ± 143.5 [1220.9 - 1792.6]	**−1.0**	**0.50**
Lateral Ventricle CSFp	1.35 ± 0.82 [0.41 – 4.48]	0.82 ± 0.41 [0.23 - 2.47]	**65.3**	**$8.\times10^{-7}$**
NACGMp	29.15 ± 2.16 [23.47 - 33.06]	29.78 ± 1.64 [26.13 - 34.20]	**−2.2**	**0.052**

F = Females, M=Males; RRMS = relapsing-remitting multiple sclerosis

EDSS= expanded disability status score

T2LL = total or whole brain T2 lesion load or lesion volume

ICV = Intracranial volume

CSF = cerebrospinal fluid

NACGMp = Normal-appearing cortical gray matter percentage

NALWMp = Normal-appearing lobar white matter percentage

Table 2

Age-adjusted Pearson linear correlation coefficient (r) and significance (p) of average qMRI metrics with disease duration (DD) in the 54 RRMS patients.

qMRI metric→	VOL		PD		T2		FA		MD		AD		RD	
	p													
Corr. with DD														
F Crtx	.078	.577	.03	.834	.145	.299	.032	.818	.364	.007	.37	.006	.359	.008
T Crtx	.145	.299	.043	.759	.187	.179	.263	.057	.328	.016	.306	.026	.337	.014
P Crtx	.15	.283	.036	.796	.148	.29	.084	.552	.342	.012	.325	.018	.351	.01
O Crtx	.088	.53	.06	.67	.174	.213	.253	.068	.03	.829	.013	.924	.057	.686
Cing gm	.241	.082	.046	.744	.319	.02	.109	.436	.388	.004	.4	.003	.378	.005
INS gm	.17	.224	.012	.933	.158	.26	.049	.727	.151	.281	.158	.258	.146	.297
HA	.093	.506	.05	.72	.312	.023	.315	.022	.36	.008	.301	.029	.38	.005
CS	.108	.441	.06	.668	.164	.241	.136	.333	.245	.078	.209	.133	.26	.06
F L wm	.447	.001	.07	.617	.232	.095	.204	.143	.241	.083	.25	.07	.233	.093
TL wm	.398	.003	.005	.972	.289	.036	.278	.044	.314	.022	.278	.044	.319	.02
PL wm	.486	*	.002	.988	.21	.131	.288	.037	.232	.095	.203	.146	.242	.08
OL wm	.111	.43	.045	.748	.153	.274	.38	.005	.197	.157	.082	.558	.242	.081
CL wm	.451	.001	.081	.566	.383	.005	.267	.054	.427	.001	.385	.004	.421	.002
INS wm	.349	.01	.164	.24	.315	.022	.092	.514	.337	.014	.308	.025	.298	.03
eCC	.231	.096	.165	.239	.383	.005	.333	.015	.435	.001	.379	.005	.439	.001
PV wm	.352	.01	.262	.059	.261	.059	.304	.027	.342	.012	.296	.032	.363	.007
THp	.144	.304	.066	.638	.288	.036	.096	.495	.136	.332	.128	.362	.136	.33
Caudate	.139	.322	.005	.974	.044	.752	.001	.997	.13	.355	.139	.321	.122	.383
Putamen	.227	.102	.053	.706	.106	.451	.089	.528	.323	.018	.231	.096	.36	.008
GP	.107	.445	.136	.333	.032	.821	.126	.37	.003	.985	.118	.399	.066	.64
HC	.038	.789	.042	.765	.323	.019	.335	.014	.379	.005	.328	.017	.397	.003
AM	.171	.222	.081	.563	.166	.234	.185	.185	.109	.435	.042	.767	.143	.306
Ac	.149	.286	.059	.672	.149	.287	.02	.886	.305	.026	.305	.026	.27	.05
aCC	.145	.3	.232	.094	.374	.006	.451	.001	.474	.0003	.437	.001	.481	.0003
maCC	.203	.144	.174	.213	.421	.002	.203	.145	.354	.009	.321	.019	.352	.01

qMRI metric→	VOL	p	PD		T2		FA		MD		AD		RD	
tCC	.261	.059	.167	.233	.44	.001	.199	.152	.354	.009	.329	.016	.348	.011
iCC	.24	.084	.078	.579	.321	.019	.248	.074	.338	.013	.282	.041	.336	.014
sCC	.186	.182	.112	.427	.267	.053	.203	.145	.328	.017	.196	.159	.328	.016

** < 0.001

Table 3

Age-adjusted Pearson linear correlation coefficient (r) and significance (p) of average qMRI metrics with whole brain lesion load (LL) in the 54 RRMS patients.

qMRI metric→	VOL		PD		T2		FA		MD		AD		RD	
	p													
Corr. with LL														
F Crtx	.126	.369	.077	.583	.335	.014	.218	.116	.534	*	.521	*	.54	*
T Crtx	.315	.022	.095	.5	.35	.01	.157	.263	.538	*	.555	*	.524	*
P Crtx	.18	.198	.085	.545	.41	.002	.003	.983	.449	.001	.442	.001	.451	.001
O Crtx	.03	.833	.092	.513	.315	.022	.133	.341	.334	.015	.302	.028	.347	.011
Cing gm	.207	.136	.103	.462	.514	*	.265	.055	.563	*	.56	*	.559	*
INS gm	.029	.834	.094	.502	.495	*	.207	.137	.547	*	.566	*	.534	*
HA	.211	.13	.167	.231	.444	.001	.421	.002	.463	*	.384	.005	.491	*
CS	.519	**	.038	.785	.148	.291	.052	.714	.399	.003	.415	.002	.374	.006
F Lwm	.454	.001	.006	.967	.67	10-7	.409	.002	.571	**	.626	***	.541	*
TL wm	.54	**	.079	.574	.653	***	.578	*	.611	**	.528	**	.625	***
PL wm	.473	**	.021	.879	.682	10-7	.483	*	.508	**	.495	**	.508	**
OL wm	.205	.141	.02	.889	.575	***	.46	.001	.447	.001	.36	.008	.471	*
CL wm	.619	***	.188	.177	.682	10-7	.51	*	.627	**	.524	***	.642	**
INS wm	.235	.09	.179	.2	.698	10-8	.32	.019	.726	10-9	.586	***	.698	10-8
eCC	.582	**	.467	*	.634	***	.466	*	.579	**	.513	***	.579	*
PV wm	.746	10-9	.463	*	.696	10-8	.54	***	.678	10-7	.618	10-6	.698	10-8
THp	.569	***	.086	.54	.381	.005	.221	.111	.299	.03	.409	.002	.221	.111
Caudate	.46	.001	.216	.121	.049	.727	.241	.082	.271	.05	.33	.016	.231	.095
Putamen	.494	***	.002	.99	.169	.227	.158	.26	.462	***	.45	.001	.409	.002
GP	.395	.003	.253	.068	.099	.479	.287	.037	.248	.074	.005	.974	.315	.022
HC	.261	.059	.168	.228	.454	.001	.458	.001	.478	***	.402	.003	.507	***
AM	.044	.756	.152	.277	.312	.023	.267	.053	.319	.02	.232	.094	.352	.01
Ac	.407	.002	.035	.806	.325	.018	.13	.354	.295	.032	.223	.108	.306	.026
aCC	.524	***	.375	.006	.648	****	.321	.019	.459	.001	.501	***	.425	.002

qMRI metric→	VOL	p	PD		T2		FA		MD		AD		RD	
maCC	.522	***	.413	.002	.599	***	.338	.013	.611	***	.587	***	.587	***
tCC	.484	***	.378	.005	.583	***	.38	.005	.533	***	.483	***	.531	***
iCC	.583	***	.555	***	.611	***	.478	***	.573	***	.438	.001	.588	***
sCC	.452	.001	.489	***	.614	***	.461	.001	.528	***	.239	.084	.58	***

** <0.001

*** <0.0001

**** <0.00001

***** <0.000001

Table 4

Age and LL adjusted Spearman linear correlation coefficient (r) and significance (p) of average qMRI metrics with expanded disability status score (*EDSS*).

qMRI→	VOLp		PD		T2		FA		MD		AD		RD	
F Crtx	.045	.75	.15	.29	.202	.15	.128	.37	.272	**.05**	.264	.058	.291	**.036**
T Crtx	.096	.50	.166	.24	.22	.12	.059	.68	.316	**.022**	.296	**.033**	.302	**.029**
P Crtx	.018	.90	.082	.56	.183	.20	.246	.079	.315	**.023**	.281	**.043**	.335	**.015**
O Crtx	.076	.59	.051	.72	.213	.13	.296	**.033**	.01	.94	.059	.67	.057	.69
Cing Crtx	.016	.91	.075	.60	.347	**.01**	.057	.69	.391	**.004**	.388	**.004**	.375	**.006**
Insular Crtx	.001	.997	.173	.22	.313	**.02**	.16	.26	.273	**.05**	.257	.066	.258	.06
HA	.051	.72	.157	.27	.278	**.046**	.235	.094	.128	.36	.012	.93	.13	.36
CS	.108	.44	.149	.29	.054	.71	.065	.65	.071	.62	.005	.97	.113	.42
FL wm	.286	**.04**	.084	.55	.232	.098	.052	.71	.018	.90	.029	.84	.032	.82
TL wm	.245	.08	.135	.34	.168	.23	.041	.77	.077	.59	.04	.78	.065	.65
PL wm	.264	.06	.018	.90	.038	.79	.005	.97	.005	.97	.022	.88	.001	.995
OL wm	.178	.21	.05	.72	.108	.45	.247	.077	.032	.82	.073	.61	.089	.53
CL wm	.28	**.045**	.034	.81	.315	**.02**	.104	.46	.289	**.038**	.25	.074	.246	.078
Insular wm	.301	**.03**	.032	.82	.197	.16	.025	.86	.187	.18	.202	.15	.12	.40
eCC	.411	**.002**	.008	.95	.326	**.018**	.058	.68	.322	**.02**	.403	**.003**	.24	.08
PVwm	.279	**.045**	.046	.75	.237	.09	.187	.18	.222	.11	.144	.31	.253	.071
Thalamus P	.155	.27	.127	.37	.147	.30	.121	.39	.093	.51	.009	.95	.083	.60
Caudate	.11	.42	.2	.17	.16	.27	.07	.6	.07	.63	.09	.53	.07	.64
Putamen	.18	.21	.14	.33	.02	.89	.01	.94	.07	.63	.00	.99	.10	.49
G. Pallidum	.03	.82	.06	.67	.09	.51	.25	.07	.02	.88	.19	.19	.14	.32
Accumbens	.16	.27	.12	.42	.23	.1	.03	.83	.09	.52	.04	.78	.14	.33
Hippocampus	.06	.68	.13	.35	.27	**.05**	.32	**.02**	.1	.49	.05	.72	.13	.34
Amygdala	.22	.12	.11	.46	.21	.14	.06	.65	.01	.97	.00	.99	.06	.69
aCC	.37	**.01**	.02	.87	.27	**.05**	.11	.42	.26	.06	.3	**.03**	.2	.16
maCC	.35	**.01**	.01	.92	.37	**.01**	.08	.58	.31	**.03**	.35	**.01**	.24	.08
bCC	.32	**.02**	.04	.75	.27	**.05**	.12	.4	.33	**.02**	.34	**.01**	.29	**.04**

qMRI→	VOLp		PD		T2		FA		MD		AD		RD	
iCC	.30	**.03**	.05	.74	.22	.11	.02	.92	.24	.09	.29	**.04**	.17	.24
sCC	.31	**.03**	.11	.43	.36	**.01**	.02	.89	.31	**.02**	.29	**.04**	.19	.18

Significant values of **$p \leq 0.05$** were bolded (not accounting for multiple comparisons)

Abbreviations in Tables 2, 3 , **4**

Quantitative MRI Metrics

VOLp= regional Volume-to-intracranial volume Percentage (Volume/ICV *100%)

PD = Proton Density (relative to accumbens)

T2 = Transverse magnetization relaxation time

FA = Fractional Anisotropy

AD, MD, RD = Axial, Mean and Radial diffusivities, respectively.

Brain Structures

gm= gray matter; wm =white matter

F, T, P, O Crtx = Frontal, Temporal, Parietal, Occipital Cortex gray matter, respectively

FL, TL, PL, OL wm = Frontal, Temporal, Parietal, Occipital Lobe white matter, respectively

Cing = cingulate, INS = Insula, HA= Hippocampus and Amygdale combined

eCC = entire Corpus Callosum. PV = periventricular WM

HC = Hippocampus, AM= Amygdala, Ac = Accumbens area

a, ma, t, i, sCC = anterior, middle anterior, truncus or body, isthmus and splenium of the Corpus Callosum, respectively.

CS = corpus striatum = Caudate + Putamen + Glopus Pallidus